Chapter 19

## El Niño and the Southern Oscillation (ENSO)

The previous chapter stressed the importance of the tropics for the coupling between ocean and atmosphere and showed how positive feedback between the sea surface temperature (SST) and the atmospheric convection zones can result in rapid magnifications of initially small disturbances. We now continue this theme and examine in detail the situation in the tropical Pacific Ocean. This region is characterized by very high sea surface temperatures and extremely low zonal temperature gradients in the west (the so-called "warm pool"; see Figure 2.5a); small SST variations in this region can grow into interannual climate variations of global proportions.

We start by looking at some observations. It is well known that climate conditions in the Australian continent vary between the extremes of devastating droughts and equally devastating floods. In eastern Australia, years of severe drought have been documented for nearly two centuries, and it has been noticed that they come at irregular intervals of a few years. We know now that they are part of a global phenomenon known as the El Niño - Southern Oscillation, or ENSO, phenomenon, which manifests itself in fluctuations of rainfall, winds, ocean currents, and sea surface temperature of the tropical oceans, and of the Pacific Ocean in particular. If these fluctuations were strictly periodic people would probably have learnt to plan for their occurrence. What makes them so difficult to cope with is their irregularity. As it is, the ENSO affects national economies often in an unpredictable manner, causing great hardship and social upheaval and at least on one occasion the downfall of a government (Tomczak, 1981a). The data shown in Figure 19.1

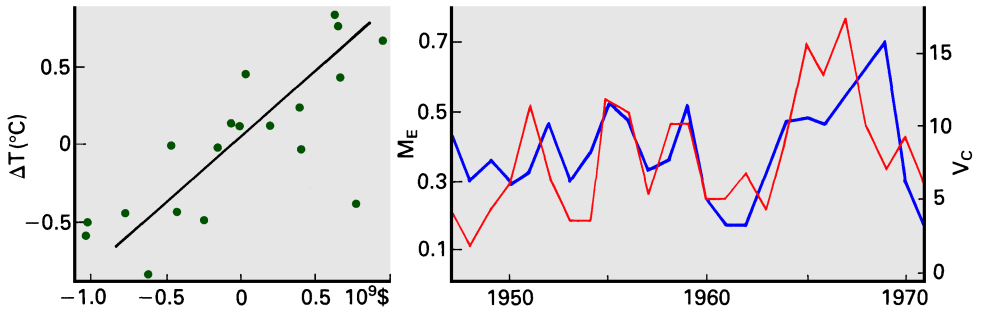


Fig. 19.1. Examples of the impact of climate variability on economic activity. (a) Anomalies of sea surface temperature (SST) in northern Australian winter (June-August, 5° - 15°S, 120 - 160°E) against variations in aggregate value of five Australian crops (wheat, barley, oats, sugar cane, and potatoes) in the subsequent summer, after removal of long-term trends due to productivity. Low SST is associated with drought; the regression line indicates a decrease of 1 billion $ for a 1°C decrease in SST. (b) Variations in wind intensity along the coast of Oregon, as measured by the mean offshore Ekman transport $M_E$ during April to September ($m^2$ $s^{-1}$per m of coastline, left scale and thin line), and variations in the catch of Dungeness crab ($V_C$, in million pounds, right scale and thick line) eighteen months later. The total catch reflects upwelling conditions remarkably well. (The time scale is correct for $M_E$ but shifted by 18 months for $V_C$.)

are only a poor indicator for this; dollar values and variations of gross national product do not convey the amount of human suffering behind them. But they indicate the magnitude and importance of the task ahead, the development of a reliable forecast of year-to-year climate variations, of which ENSO variations are a major part.

## The Southern Oscillation

When Sir Gilbert Walker became Director-General of Observatories in the British colony of India in 1904 he set himself the task of trying to predict variations in the Indian monsoons and related droughts. To this end he started a project to examine global records of sea-level pressure, temperature, rainfall, and other variables from around the world. These records had been collected in the colonies of the major European powers and accumulated over some decades. Within each year of record, Walker calculated the seasonal averages for pressure and rainfall at each station. The averages would differ from year to year; but the patterns of the differences turned out to be similar over wide regions of the globe. An example is shown in Figure 19.2, which applies the technique of a twelve-month running mean to observations of air pressure at Darwin and of rainfall over the equatorial mid-Pacific Ocean (thus giving values for every month rather than seasonal values only, as in Walker's original method). The similarity in pattern comes out clearly.

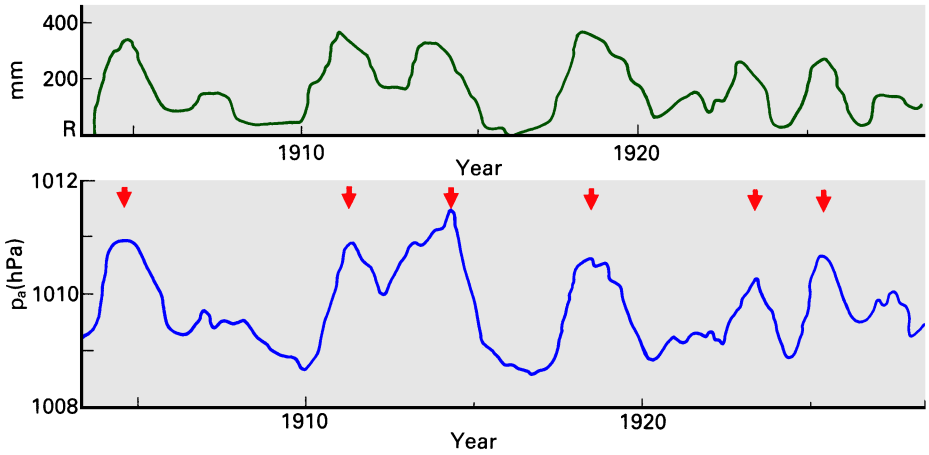


Fig. 19.2. Twelve-month running mean of air pressure $p_a$ for Darwin (bottom) and of average rainfall $R$ at a series of islands in the central equatorial Pacific Ocean between 160°E and 150°W (top). Arrows identify ENSO events for comparison with Fig. 19.4.

Walker plotted world maps of these differences and found that they were dominated by a single spatial pattern. Figure 19.3 shows a modern compilation of this spatial pattern, using objective mathematical methods. The "Southern Oscillation Index" used for the figure is a composite number derived from observations of air pressure at sea level for Cape

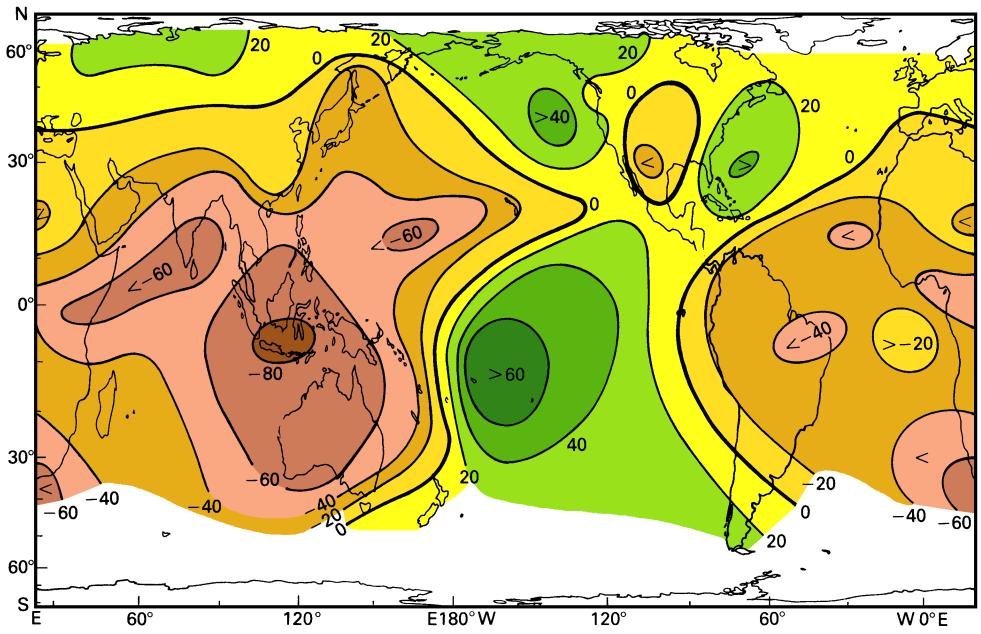


Fig. 19.3. Correlation (%) between air pressure at sea level and the Southern Oscillation Index (for explanation of the index, see text) for December - February. Adapted from Wright (1977).

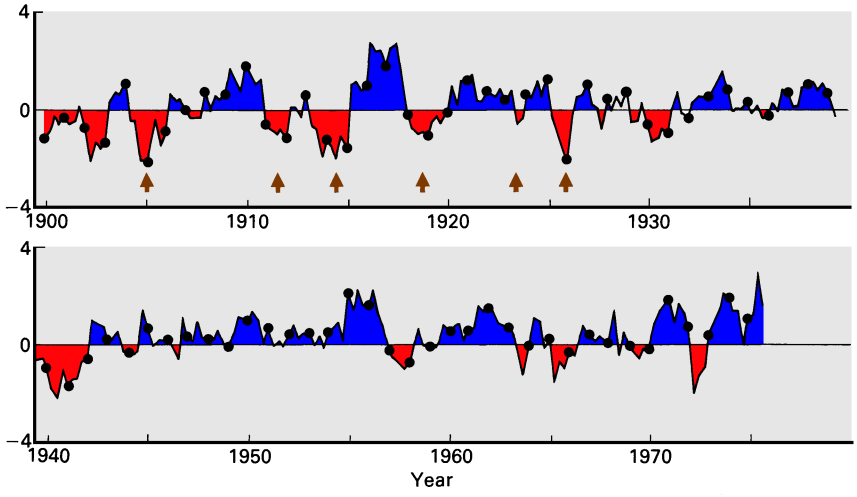


Fig. 19.4. Time series of seasonal values of the Southern Oscillation Index in units of one standard deviation from the mean. Seasons are defined February - April (identified by the dots on the curve), May - July, August - October, and November - January. For an explanation of the index, see text. Arrows identify ENSO events for comparison with Fig. 19.2.

Town, Bombay, Djakarta, Darwin, Adelaide, Apia, Honolulu, and Santiago de Chile. (This is not the only definition of the Index in use; a more commonly used simpler version uses the difference in air pressure at sea level between Tahiti and Darwin). Its time history during the present century is given in Figure 19.4 (which, by comparison with Figure 19.2, shows that air pressure at Darwin contributes to the Southern Oscillation Index (SOI) in the inverse sense: Darwin air pressure is low when the SOI is high, and high when the SOI is low). The correlation map indicates a cellular structure of the air pressure field in the tropics, with high pressure in the central South Pacific Ocean and low air pressure over Australia, south-east Asia and India, central and southern Africa, and South America when the SOI is high. As the SOI reverses from positive to negative (as occurred, for example, from 1971 to 1972; see Figure 19.4), so does the spatial pattern, the highs turning into lows and the lows into highs. When searching for a name for the phenomenon, Walker compared it with the more regular seasonal variations of air pressure over the North Atlantic Ocean (the natural point of reference for a colonial officer of the British Empire) and chose the term "Southern Oscillation" for what is essentially a phenomenon of the tropics. His choice of name has now been accepted by meteorologists in both hemispheres.

## El Niño

One of the richest fishing regions of the World Ocean, the South Pacific coastal upwelling region along the coast of Peru, Chile, and Ecuador, occasionally experiences an influx of warm tropical water which suppresses the upwelling of nutrients. The *anchoveta*, which inhabit these waters in their millions forming the nutritional basis for a huge bird population and the stock for an important fish meal industry, depend on the supply of nutrients into the surface layer. They avoid the warm nutrient-poor water, which causes mass mortality amongst the birds (Figure 19.5). If the extent of the tropical influx is very severe, mass mortality can occur among the fish as well; hydrogen sulfide from decaying fish has been known to blacken the paint on ships in Callao harbour. The high temperatures along the South American coast last for about a year or more before conditions return to those which prevailed before the influx of tropical water.

The phenomenon has become known as El Niño, a term originally used by the fishermen of the Peruvian port of Paita to describe an influx of warm but nutrient-rich coastal water from the Gulf of Guayaquil (Tomczak, 1981b; Philander, 1990). This influx, which heralded good catches, usually occurs in December, which the fishermen (and millions of people in Christian communities around the world) associate with Christmas. The choice of "el niño" (the child) for an oceanic phenomenon as welcome and awaited as the birth of Christ appears sensible. Unfortunately, the influx of tropical nutrient-poor oceanic water associated with the suppression of the upwelling also manifests itself in a rise of surface temperature in December. When oceanographers began studying the phenomenon they failed to differentiate between the two different advective processes and adopted the local term El Niño for an oceanic phenomenon of much larger scale and of devastating effects for the fishermen.

Although oceanographers have been aware of the phenomenon for many decades (e.g. Sverdrup *et al*., 1942), it was not until 1966 that Bjerknes (1966, 1969), a meteorologist who had become interested in ocean dynamics, pointed out the close relation

between El Niño and the Southern Oscillation. As an illustration from modern data, Figure19.6 shows correlation coefficients between sea surface temperature and the Southern Oscillation Index in December - February. It is seen that sea surface temperature is low when the SOI is high (negative correlation) in a broad region of the east Pacific Ocean surrounding Peru; but it is also negative (at this time of year) in the far western Pacific, most of the Indian, and the central South Atlantic Ocean. It is evident that the phenomenon is not restricted to the south Pacific coastal upwelling region but is of global scale.

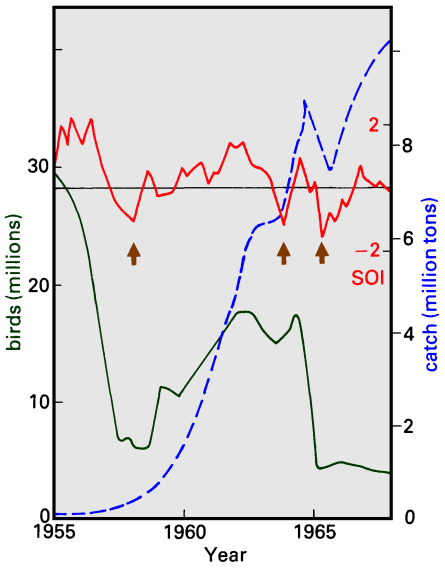


Fig. 19.5. An example of the effect of El Niño on the biosystem in the upwelling region along the coast of Chile and Peru. annual catch of *anchoveta* (dotted line), number of sea birds, and Southern Oscillation Index (SOI). El Niño events are indicated by arrows on the SOI curve. The 1957 El Niño decimated the bird population. The subsequent build-up of an *anchoveta* fishery resulted in a new competitor and prevented the bird population from recovering to pre-1957 levels. The 1963 and 1965 El Niños affected both competitors, though the bird population suffered more severely. The fishery eventually collapsed to below 3 million tons as a result of overfishing and the 1973 El Niño (see Tomczak (1981a) for more details).

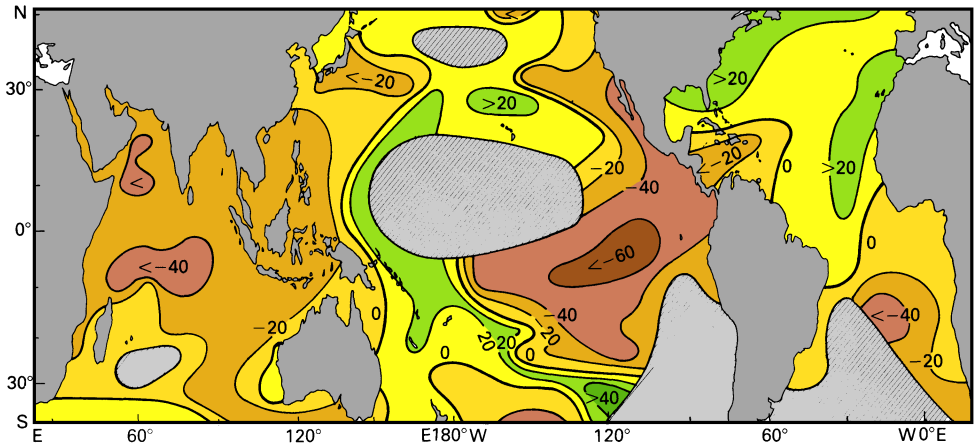


Fig. 19.6. Map of the correlation (%) between sea surface temperature and the Southern Oscillation Index for the December - February season. Data were obtained from merchant vessels along the major shipping routes. Shading indicates regions with no data due to a lack of shipping activity.

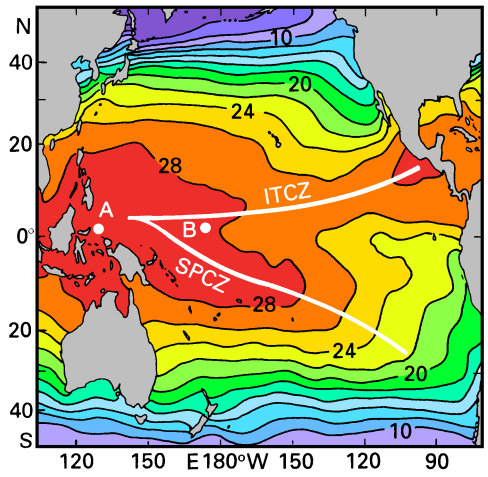


Fig. 19.7. The positions of the Intertropical Convergence Zone (ITCZ) and the South Pacific Convergence Zone (SPCZ) in relation to the annual mean sea surface temperature (°C), based on Levitus (1982). See text for the significance of locations *A* and *B*.

The combined process of El Niño and the Southern Oscillation has become known as ENSO, and the suppression of upwelling in the east accompanied by a drought in the west is now called an *ENSO event*. During the last two decades, with the availability of rainfall estimates over many years (derived from the outgoing long wave radiation measurements; see Chapter 18) and with improved knowledge of the SST distribution, it has become clear that ENSO is an instability of the coupled ocean - atmosphere system in the tropics. An indication of the effectiveness of the coupling can be seen with the intense rainfall bands of the ITCZ and SPCZ and the associated SST maxima; both are consistently found in close proximity. In an ENSO event, the entire Pacific air - sea system - rain bands and their associated winds, wind-driven currents and SST patterns - all move eastwards together, and the apex formed by the ITCZ and SPCZ in the west, which before the ENSO event was located at point *A* of Figure 19.7, moves to the dateline (point *B*). On average, the rainfall and SST maxima remain so close to one another that it is not possible to tell through the noise of shorter timescale rainfall variations whether the SST changes are causing the changes in rainfall or vice versa. The rainfall in the central Pacific Ocean strengthens, so that the convection system there competes successfully with the neighbouring convection systems for a while, suppressing their rainfall. Severe drought in Australia, Indonesia and to a lesser extent South Asia results. The centre of convection stays near the central equatorial Pacific Ocean (point *B* in Figure 19.7) for a year or more, before returning to the more common location in the far west (point *A*), bringing the ENSO event to an end. More detailed analysis of the time development of an ENSO event requires some elementary knowledge of tropical ocean dynamics, which we will introduce in the next few paragraphs.

## Some aspects of ENSO dynamics

Understanding the evolution of an ENSO event begins with an understanding of the evolution of the SST field. Many factors can influence the sea surface temperature. A change in wind speed affects evaporative heat loss; wind stresses create Ekman drifts, which advect surface water horizontally, and also create Ekman pumping, which changes the

deeper density field and therefore the temperature of the water available for upwelling (a particularly important mechanism for SST change in the equatorial east Pacific Ocean, as we shall see). The changed density field alters the geostrophic flow, which also contributes to advection; and finally winds also provide the mechanical energy for stirring deeper water into the mixed layer. A seventh important mechanism for SST change is that due to changes in cloud cover. This plethora of different mechanisms for SST change has meant that, despite considerable progress in recent years, it has not yet been possible to identify a clearly-defined, single mechanism as the trigger for ENSO events. Indeed, there may not be a single dominant mechanism.

However, there is general agreement on one point: Westerly wind bursts in the western Pacific Ocean, i.e. reversals of the general Trade Wind pattern, seem to be a necessary ingredient of the initialization process for an ENSO event. The winds in the equatorial western Pacific Ocean are usually very light; but occasionally an outbreak of westerly winds occurs, perhaps for a week or more at a time, over thousands of kilometers - sometimes along the entire 4000 km stretch from Indonesia to about 170°W. These bursts are linked at their eastward end with pairs of low pressure cells that eventually grow into tropical cyclones (or typhoons, as they are known in the northern hemisphere). Figure 19.8 shows an example of such a situation. The two low pressure cells of 18 May 1986 later separated to lead independent lives as tropical cyclones on either side of the equator.

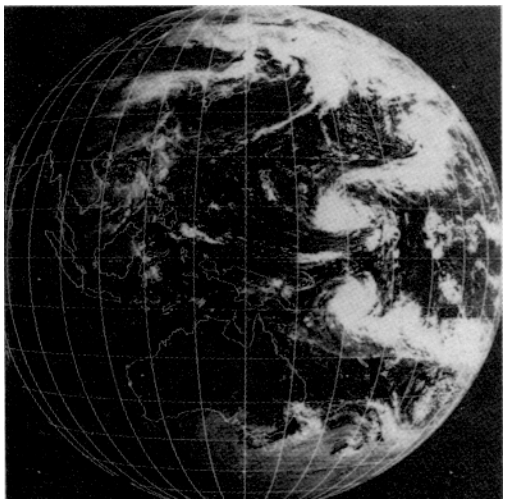

Fig. 19.8. (Right) Cloud cover over the western Pacific Ocean as observed by satellite on 18 May 1986, indicating a tropical cyclone pair in formation near 160°E. (The latitude/longitude grid shows every 10°; the centre longitude is 140°E.) Note the westerly winds at the equator.

These westerly wind bursts are important for setting in train wave motions characteristic for the equatorial region (Figure 19.9). They literally blow surface water eastward along the equator. Because during westerly winds the Ekman transports are directed towards the equator, these wind bursts also deepen the thermocline on the equator. The equatorward Ekman transports are generally confined to the band between about 5°N and 5°S, so the thermocline shallows near 5° - 7° N or S. A strong westerly burst can create thermocline disturbances such as sketched in Figure 19.9b within a few days. These disturbances then begin to move, through the action of equatorial wave dynamics.

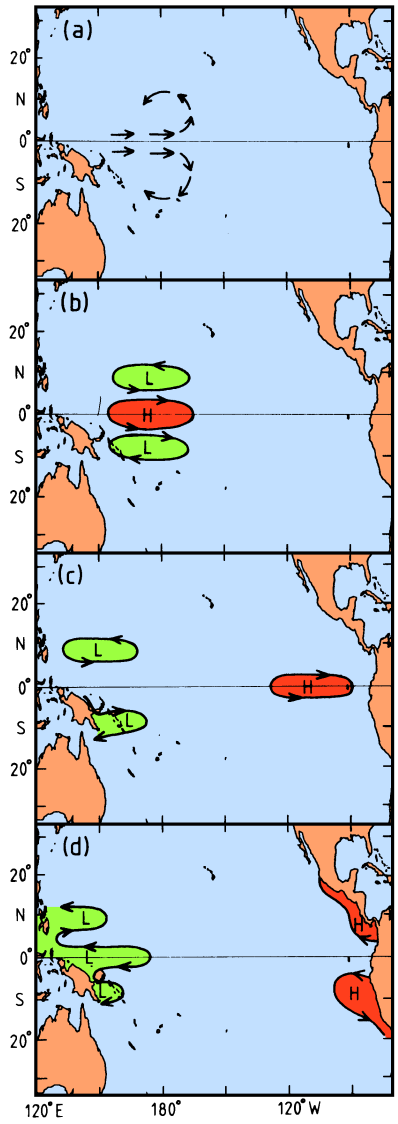


Fig. 19.9. Sketch of wave propagation during an ENSO event. (a) Wind stress *anomalies* associated with a typical westerly wind burst, (b) distribution of thermocline depth anomalies a few days after the westerly wind burst; Ekman convergence has piled thermocline water up near the equator, at the expense of off-equatorial regions, (c) distribution of thermocline depth anomalies about a month after a westerly wind burst; the off-equatorial regions of shallowed thermocline have moved slowly westward as Rossby waves, while the equatorial region of deepened thermocline has moved rapidly eastwards as an equatorial Kelvin wave, (d) distribution of thermocline depth anomalies about two months after a westerly wind burst; the Rossby waves have reached the western boundary, propagated equator-ward and created a new (upwelling) equatorial Kelvin wave emanating from the western boundary; the first equatorial Kelvin wave has reached the eastern boundary, spread poleward and created new Rossby waves that are starting to propagate slowly back into the Pacific Ocean.

The regions of shallowed thermocline near 5-7°N and 5 - 7°S at first move westward, by the Rossby wave propagation mechanism discussed in Chapter 3. It can be shown that eqn (3.11), which gave us the Rossby wave propagation speed as a function of latitude in a $1^1/_2$ layer ocean, is no longer valid at these short distances from the equator; nevertheless, it gives a useful first approximation. For typical thermocline depths $H$ of 150 m and a density ratio $\Delta\rho/\rho = 0.004$ the shallow thermocline regions move west at 6°N or S at a speed of about 0.3 m $s^{-1}$, taking a few months to reach the western boundary from the dateline, as sketched in Figure 19.9c.

Figure 19.9c shows also that the equatorial thermocline depression has moved rapidly eastward. This movement occurs at a speed of $c_g = (g\ \Delta\rho\ H\ /\ \rho)^{1/2}$, or about 2.5 m $s^{-1}$,

and is due to the action of equatorial *Kelvin waves*. The principle of a Kelvin wave propagating along the equator is illustrated in Figure 19.10a. Note that an equatorial Kelvin wave can only move eastwards. Several clear examples of Kelvin wave generation by westerly wind bursts have been seen on Pacific tide gauge records. They travel with little dissipation over the entire width of the Pacific Ocean, about 10 - 20% faster than the predicted speed; the excess speed is due to advection by the Equatorial Undercurrent.

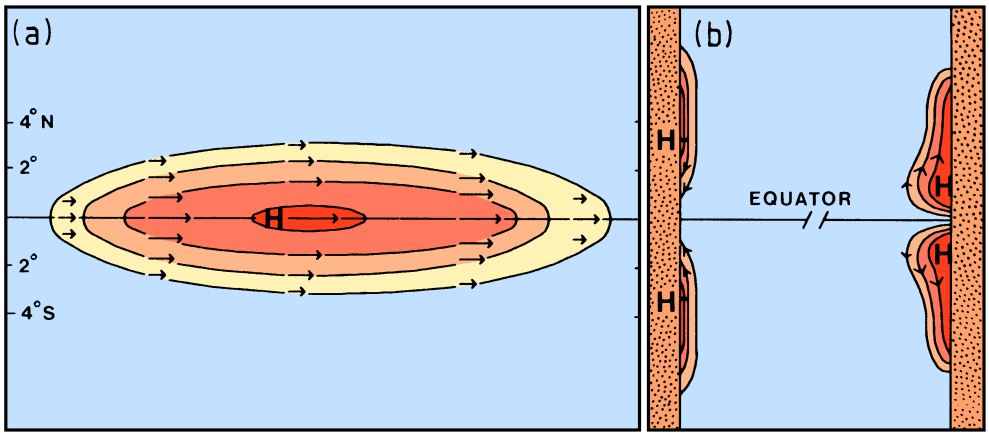


Fig. 19.10. Sketch of Kelvin wave dynamics. (a) For an internal equatorial Kelvin wave, in a $1^1/_2$ layer ocean; contours indicate upper layer pressure or thermocline depth, arrows show flow direction. An isolated thermocline depression spans the equator; flow is purely zonal, in geostrophic balance and thus eastward on both sides of the equator. This removes thermocline water from the western end of the region and deposits it at the eastern end, resulting in eastward movement. (An isolated patch of *shallow* thermocline also moves eastward, though the currents and pressure gradients both have the opposite signs); (b) for internal Kelvin waves along meridional coastlines. The pressure gradients in the offshore direction are in geostrophic balance; on the western side this implies equatorward flow. This removes thermocline water from the poleward end of the region and deposits it at the equatorward end, resulting in equatorward movement. Rossby wave action keeps these waves tightly confined to the western boundary, i.e. they are disturbances of the western boundary current. Similarly, along the eastern boundary flow is poleward; this removes thermocline water from the equatorward end of the region and deposits it at the poleward end, resulting in poleward movement. In this case the patches can also propagate slowly westward through Rossby wave propagation, resulting in broadening of the pattern, especially near the equator.

After another month or so the patch of shallow thermocline has reached the western boundary and has started to produce a disturbance in the western boundary currents there. This occurs primarily equatorward of the original patch of shallow thermocline (Figure 19.10b). These equatorial disturbances in turn generate new equatorial Kelvin waves which propagate rapidly eastward, this time involving an uplifting of the thermocline (the "nose" of shallow thermocline emanating from the west in Figure 19.9d).

The reflected Kelvin waves have longer period than the westerly wind burst that gave rise to them, and correspondingly lower amplitude. Meanwhile the first equatorial Kelvin wave has reached the east Pacific coast and propagated poleward as two coastal Kelvin waves. These in turn generate new - though diffuse - Rossby waves that radiate away from the eastern boundary (Figure 19.10b).

It can be imagined that these changes in thermocline depth induced by a westerly wind burst will affect SST in rather complex ways, far beyond the winds that produce them. The initial downwelling Kelvin waves of Figure 19.9b have two effects in the east Pacific Ocean. First they depress the thermocline, so that — even though upwelling favourable winds are still active — the upwelled water is substantially warmer than before. (This effect is not as strong in the central west Pacific Ocean, where the upwelled water is quite warm both before and during the passage of the Kelvin wave.) Secondly, the associated eastward currents point down the mean zonal SST gradient in the equatorial Pacific Ocean; i.e. horizontal advection also results in warming. As described in Chapter 18, Ekman drifts carry the warmer upwelled water poleward, so the effects on SST extend substantially further from the equator than the 300 km width of the original Kelvin wave. When the coastal Kelvin waves pass along the region of very shallow thermocline next to the Peru coast, they cause the increases in SST associated with an El Niño. The Rossby waves reflected off the eastern boundary in Figure 19.9c probably also play a role in SST change.

## Anatomy of an ENSO event

This very brief summary of equatorial dynamics and our qualitative understanding of the competition between tropical convection cells from the last chapter allows us to investigate the development of a typical ENSO event in some detail. Before entering the discussion it is useful to define some terms. The time history of the Southern Oscillation Index (Figure 19.4), which is low during ENSO events, tells us that ENSO years are significantly less frequent than non-ENSO years. Distributions of oceanic or atmospheric parameters drawn from long-term annual means (such as the SST map of Figure 19.7) therefore reflect conditions during non-ENSO years. Some scientific publications and many press and television reports therefore often refer to the non-ENSO situation as the "normal" situation. From the previous discussion it should be clear that ENSO events are not abnormalities; they are basic elements of the coupled ocean - atmosphere system. Labelling a particular set of years as normal is therefore not justified. This fact has become more and more accepted in recent years, and definitions such as non-ENSO mean, ENSO-mean, pre-ENSO mean, and post-ENSO mean have found more widespread use. They refer to average conditions during years with comparable SOI values. An ENSO-mean, for example, is computed from data for all years with an SOI minimum; the non-ENSO mean would then be computed from data for all remaining years. A pre-ENSO mean uses only data from years preceding ENSO years, while a post-ENSO mean results from data for years following ENSO years. More recently, years with unusually high SOI values, which represent a particularly strong "run" of the feedback loop when the centre of high SST is at point *A* of Figure 19.7, have become known as "La Niña" years (the girl, as opposed to the strict meaning of El Niño, the boy). Whether this term will become generally accepted remains to be seen.

The existence of a positive feedback loop infers that the steady state which corresponds to the long-term mean distributions of the oceanic and atmospheric parameters is rarely, if ever, realized. The combined ocean - atmosphere system is continuously changing, in response to the positive feedback described in Chapter 18. What remains to be discussed is how the system changes from one operational state of the feedback to the other, and why the ENSO state is less frequent than the non-ENSO state. The answer to this question lies in a closer study of the time evolution of an ENSO event. Because individual ENSO events vary widely in intensity and duration, the best data set to produce a somewhat general answer is a "composite" event, i.e. the pattern which shows up in the pre-ENSO, ENSO, post-ENSO, and non-ENSO means. The data base required for such an undertaking has become available over the last three or four decades and was strengthened significantly through an international research programme designed to study ENSO dynamics. The programme, known as TOGA (Tropical Ocean, Global Atmosphere), began in 1985 and will continue into 1994 as part of the World Climate Research Programme (WCRP).

For the purpose of this description, we follow Rasmusson and Carpenter and divide the composite ENSO event into five "phases", the antecedent, onset, peak, transition, and mature phases. Figure 19.11 identifies the phases in relation to the composite ENSO year and the rainfall history at two island locations. It should be noted that there is much variability between different ENSO events, and the composites discussed below are not very useful as a practical forecasting tool. Nevertheless, they provide a frame of reference for studying in broad outline what might be happening during an ENSO event.

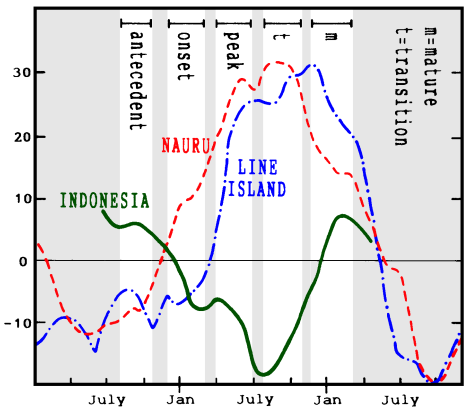


Fig. 19.11. Time development of rainfall, expressed in a rainfall index, in Indonesia, near Nauru (167°E), and in the Line Islands (near 160°W), for the composite ENSO event. Antecedent: August - October of pre-ENSO year; onset: November - January; peak: March - May; transition: August - October; mature: December - February of post-ENSO year. All values are three month running means. Note the out-of-phase relationship between Indonesian and Nauru rainfall anomalies, and the eastward propagation of the rain anomaly from Nauru to the Line Islands.

Figure 19.12 shows *anomalies* of near-surface wind vectors and SST for the antecedent phase, in August - October preceding ENSO. The Southwest Monsoon is still active at this time of year, and is stronger than usual, drawing moist air from the Pacific Ocean and thus causing the particularly strong Trades seen in the western equatorial Pacific region. SST values are slightly below the non-ENSO average across most of the equatorial Pacific Ocean, but slightly higher SST occurs near Indonesia and Papua New Guinea, (*A* in Figure 19.7). Because the mean SST maximum in Figure 19.7 is so broad, this implies an absolute SST maximum near *A*. Figure 19.11 shows that the high SST near *A* (Indonesia)

is accompanied by high rainfall anomalies there; rainfall is below average at *B* (near Nauru, 170°E; Figure 19.11) at this time.

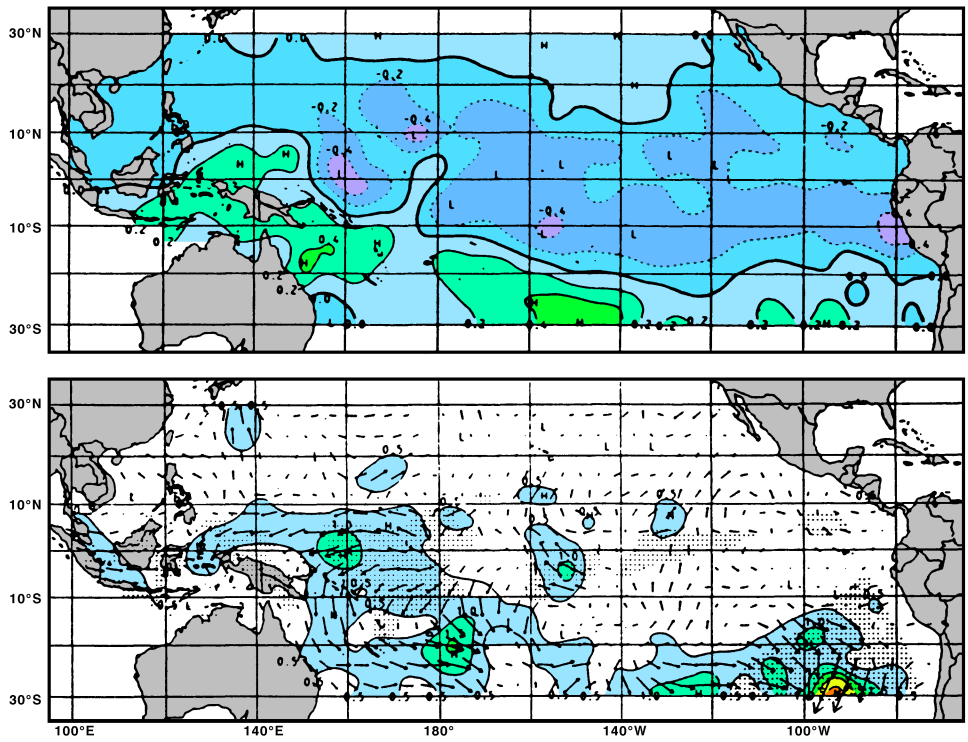


Fig. 19.12. SST anomaly (°C) and wind anomaly (m $s^{-1}$), during the antecedent phase of ENSO (August - October preceding the ENSO year). The magnitude of the wind anomaly is indicated by arrow length and also contoured in 0.5 m $s^{-1}$ intervals. Shading indicates regions where fewer than 10 observations were available in a 2° square. From Rasmusson and Carpenter (1982).

The onset phase, seen in Figure 19.13, corresponds to November - January preceding the ENSO event. The sun has crossed the equator, and the Australian summer monsoon has started. Wind anomalies have reversed in the equatorial western Pacific region and just north of Australia. Because the monsoon winds reverse seasonally, this in fact represents a strengthening of the Australian summer monsoon winds. This is not unusual, given that the preceding Asian summer monsoon was strong; a strong Asian monsoon is usually followed by a strong Australian monsoon (Meehl, 1987). The slight cooling of SST of about 0.4°C for the Indonesian region is probably due to excess evaporation, caused by the stronger than usual Australian monsoon winds. There is also a clear warming of about the same amount near 170°E (point *B* in Figure 19.7), and strong rainfall has started here (Figure19.11). Rain has correspondingly decreased near *A*. Once again, inspection of Figure 19.7 shows that these small changes in SST imply substantial shifts of the

position of the absolute SST maximum eastward towards *B*. The strengthening of the westerlies east of Papua New Guinea is in fact due to an increased frequency of westerly wind bursts. An indication of these bursts can be seen in the composite mean as well (Figure 19.13): the wind anomalies near 170°E show a tendency for tropical cyclone pair formation near 170°E (anti-clockwise north, clockwise south of the equator).

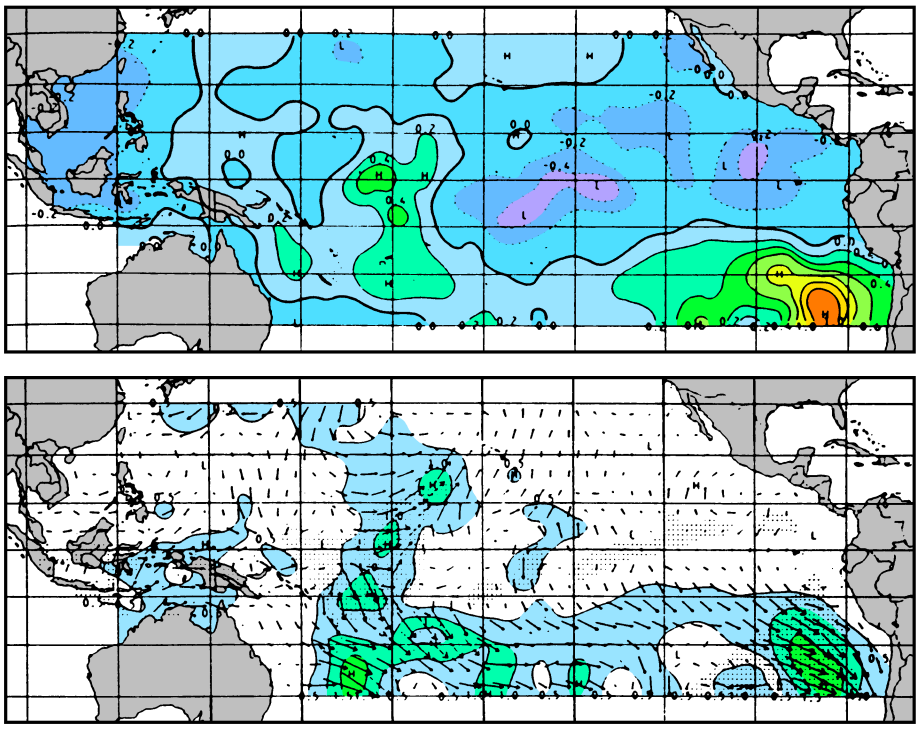

Fig. 19.13. SST anomaly (°C) and wind anomaly (m/s), during the onset phase of ENSO (November - January). For details see Fig. 19.12. From Rasmusson and Carpenter (1982).

What appears to be happening at this time of development of an ENSO event is that, associated with the strong Australian monsoon, a new convection centre forms near *B*. It competes with the more usual convection centre near *A*, sucking westerly winds towards it. We have noted that the very small SST changes from Figure 19.12 to Figure 19.13 are in fact enough to displace the very broad SST maximum from near *A* in Figure 19.7 to near *B*, so the new convection centre near *B* is consistent with the principle that convection over the Pacific Ocean follows SST maxima. Note that mean rainfall west of the date line is uniformly large (about 3 m per year from Indonesia to Nauru), so a modest fractional change in rainfall at either place is a very big change in absolute terms. The reduction of rain over Indonesia and accompanying increase over Nauru is apparent in Figure 19.11.

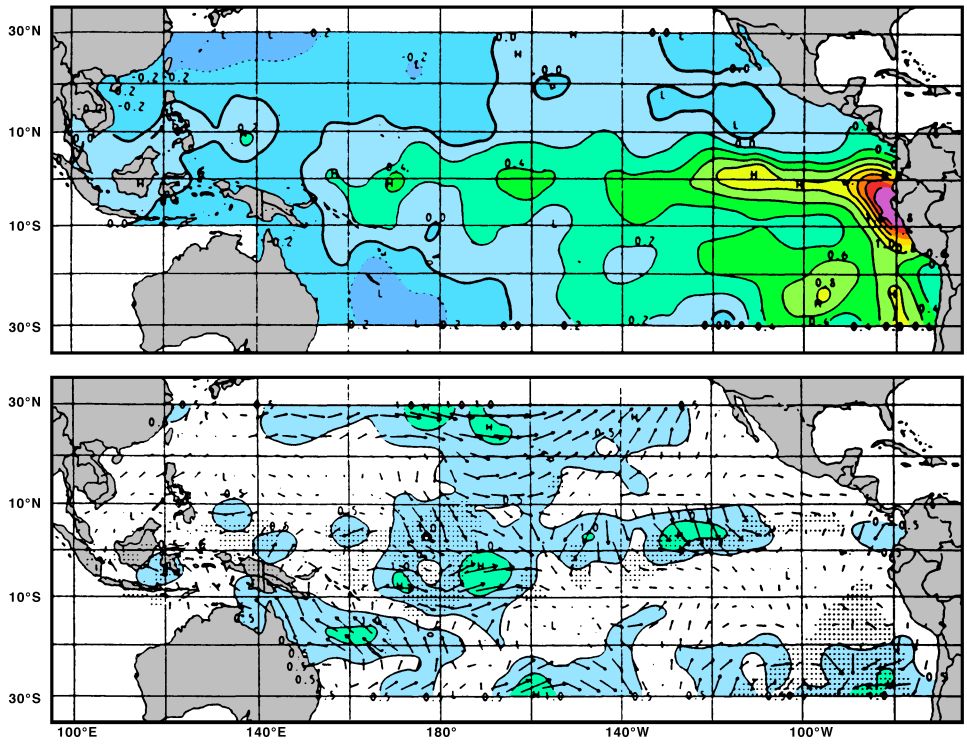


Fig. 19.14. SST anomaly (°C) and wind anomaly (m/s), during the peak phase of ENSO (March - May). For details see Fig. 19.12. From Rasmusson and Carpenter (1982).

The westerly wind anomalies in the western Pacific region of Figure 19.13 continue weakly into the peak phase of March - May, and they evidently drive downwelling equatorial Kelvin waves. The effect of these is evident in Figure 19.14; a marked warm SST anomaly has developed near South America. As explained in the preceding section, the Kelvin waves have a stronger effect on SST in the shallow thermocline of the east Pacific than in the central and west Pacific Ocean. In contrast, the small warming in the central Pacific Ocean in Figure 19.13 is probably largely due to horizontal advection.

On the basis of competition between convection centres, one might expect the centre near *B* of Figure 19.7 to "run away" after its formation. Curiously, however, this does not happen between November - January and March - May. Perhaps the reason is that the most active convection has moved with the SST to be well south of the equator during late southern summer, i.e. from February through April. The rainfall maximum near Nauru moves further east, to the Line Islands, during this period.

However, around May - June of an ENSO year when the Southern Hemisphere convection dies and a new Southwest Monsoon begins, drastic changes occur in the Pacific circulation (Figure 19.15). By August - October, violent westerly wind bursts are occurring, and SST increases throughout the east and central Pacific; the SST is reduced near Indonesia, and Indonesia and Australia experience their greatest drought intensity.

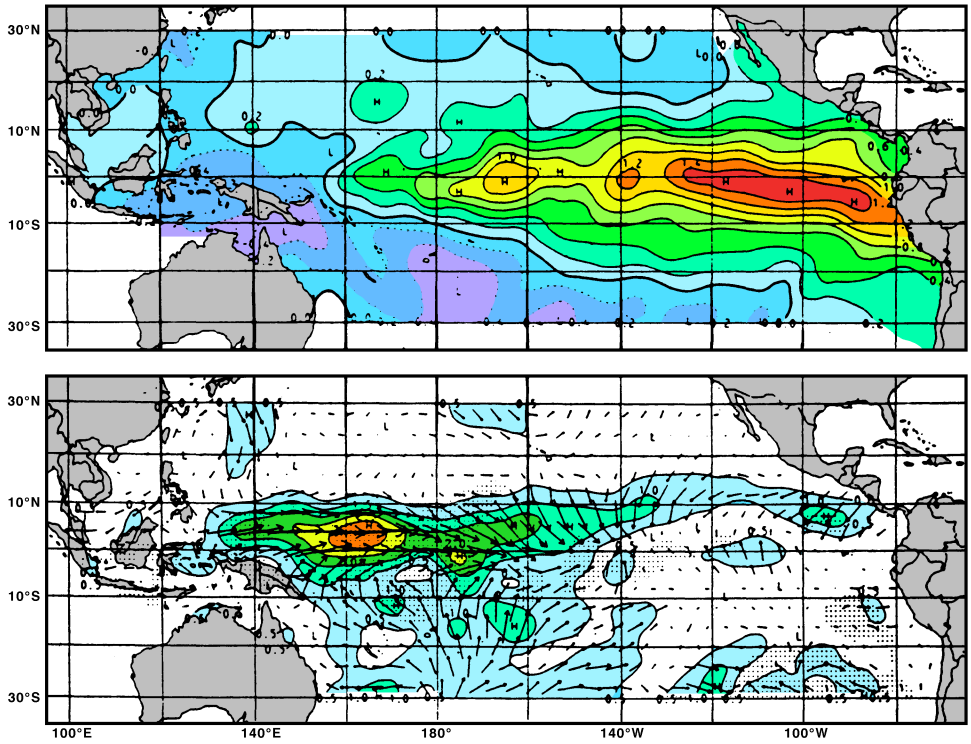


Fig. 19.15. SST anomaly (°C) and wind anomaly (m/s), during the transition phase of ENSO (August - October). For details see Fig. 19.12. From Rasmusson and Carpenter (1982).

The ENSO event usually does not break until the next change of season (December - February following El Niño), when the winds are disturbed throughout most of the Northern Hemisphere over the Pacific Ocean (Figure 19.16). A significant positive SST anomaly develops in the South China Sea and the Indonesian waters, attracting the winds from the far western Pacific Ocean which begin to blow strongly towards it, breaking the drought there, and the Trades are strong again in the west Pacific region. The east Pacific SST anomaly dies shortly thereafter.

The above description of an ENSO event places strong emphasis on the small SST anomalies in the western Pacific rather than the much more dramatic ones in the eastern Pacific Ocean, because they shift the SST maximum and hence the convection patterns to the central Pacific region. Strong support for the relative importance of the small SST anomalies in the west for ENSO comes from sensitivity tests with atmospheric models which show that a change of SST in the east affects the wind field much less than a corresponding SST change in the west. This suggests that our skills in predicting ENSO events should be closely tied to our ability to forecast very small SST changes in the western Pacific Ocean. In this region, as we have seen, the equatorial Kelvin waves do not play a dominant role in SST change; local changes in surface heat fluxes — solar radiation and evaporative heat loss — are sufficient to account for the observed SST changes in the

west Pacific Ocean. However, we are then confronted with a data quality problem. For example, the amount of heat needed to generate the 0.4°C warming in the top 50 m or so near *B* at the start of an ENSO event is only about 10 W $m^{-2}$. As was noted in the last chapter, the algorithms used to estimate heat fluxes currently have errors of substantially more than this. Hence improvement of heat flux algorithms has become a primary goal of ENSO research. It has already been shown that latent heat loss at low wind speeds has been seriously underestimated by some commonly used algorithms (Godfrey *et. al.*, 1991) and that inclusion of low-wind evaporation in some atmospheric circulation models radically improves their representation of the monsoons. The mixing of cool water into the surface mixed layer is certainly crucial in the east Pacific and can also easily make significant contributions to SST change in the west Pacific Ocean, so improvement of mixing algorithms is also a high priority for ENSO research.

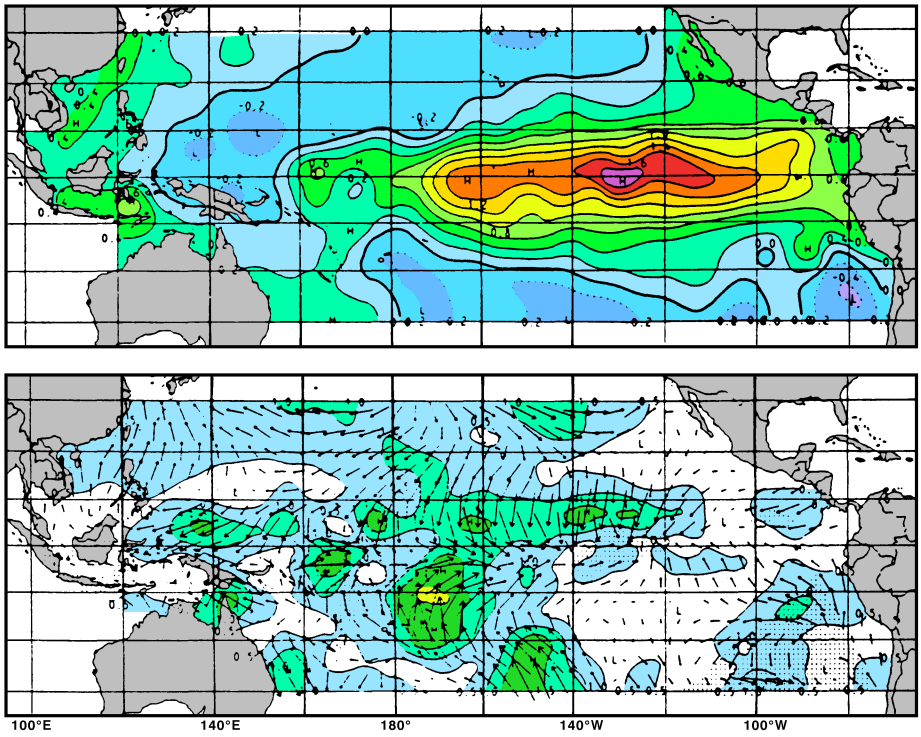


Fig. 19.16. SST anomaly (°C) and wind anomaly (m/s), during the mature phase of ENSO (December - February of the year following ENSO). For details see Fig. 19.12. From Rasmusson and Carpenter (1982).

The possibility that ENSO events and other movements of tropical convection systems might be accessible to reliable forecasting one or more seasons in advance has led to new demands on the climate observation network. This need led to the TOGA programme already mentioned earlier, which set itself the goal to "gain a description of the tropical

oceans and the global atmosphere as a time dependent system in order to determine the extent to which the system is predictable on time scales of months to years and to understand the mechanisms and processes underlying its predictability". This aim is tackled with a variety of instrumentation (Figure 19.17 shows some components of the station network in the Pacific Ocean; others include island tide gauge installations and oceanographic satellites). TOGA is increasingly seen as a forerunner of a permanent oceanic observation network analogous to the network of meteorological observation stations on land. As in meteorology, success in forecasting climate variability will be achieved by transmitting the data to information processing centres in real time and assimilating them into numerical models of the oceanic and atmospheric circulation. The planning for the Global Ocean Observing System (GOOS) began in 1992.

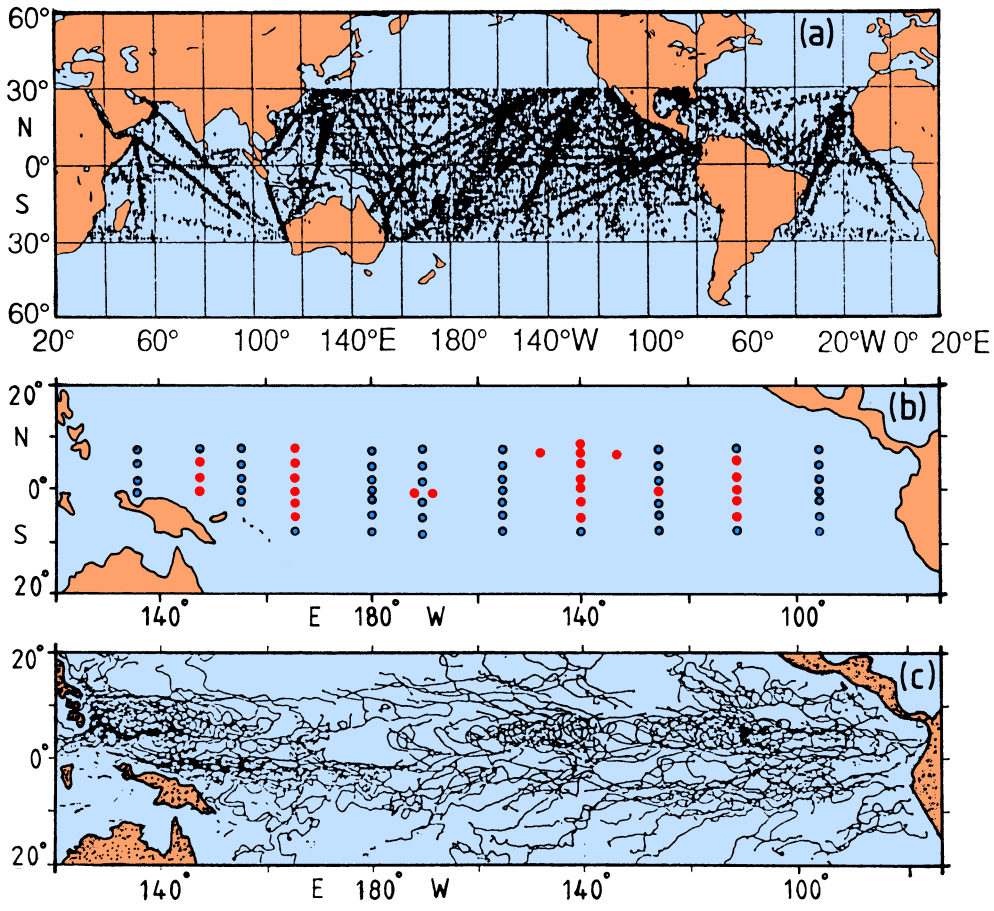


Fig. 19.17. Some of the observation components of TOGA. (a) Station positions where temperature profiles for 0 - 450 m depth, using expendable instrumentation, were obtained by merchant vessels during 1987; (b) existing (dots) and planned (1994, circles) arrays of current meter moorings; (c) trajectories of TOGA surface drifters for July 1988 - February 1990.

## Interannual variability of the equatorial Atlantic Ocean

In contrast to the Pacific Ocean, interannual variability in the equatorial Atlantic Ocean is much weaker than its strong seasonal changes. The sea surface temperature along the equator is mainly controlled by advection, and seasonal changes in the current field result in a temperature change of 6 - 8°C at the surface. In comparison, the largest documented interannual temperature change did not exceed 4°C. Nevertheless, when it is recalled that the seasonal upwelling along the coast of Ghana and Ivory Coast is the result of remote wind forcing and Kelvin wave propagation along the equator (Figure 14.20), it is seen that the El Niño mechanism is equally important to the Atlantic as to the Pacific Ocean. It plays a major role in the seasonal behaviour of the tropical ocean, and it appears to be responsible for occasional anomalous warmings of the water along the equator.

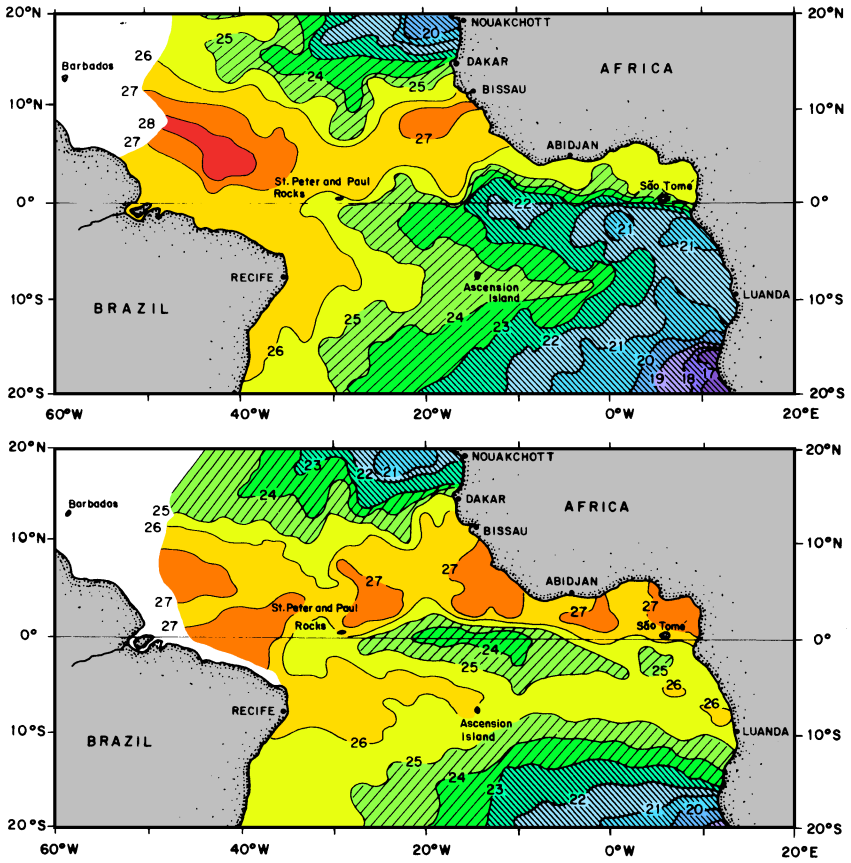


Fig. 19.18. Sea surface temperature (°C) in the tropical Atlantic Ocean. (top) June 1983, (bottom) June 1984. From Philander (1990).

Figure 19.18 shows the sea surface temperature for June 1983 and twelve months later. While temperatures in the two upwelling regions outside the 20°S - 20°N equatorial belt showed little change over the period, the water within 500 km either side of the equator east of 15°W was anomalously cold in 1983 and anomalously warm in 1984. The 1983 situation was accompanied by dry conditions in northeastern Brazil, strong equatorial Trades, and a continuation of strong upwelling in the northern part of the Benguela Current upwelling system (which usually retreats southward during this time of year). In the following year, westward flow in the equatorial current system was nearly halted, and an intrusion of tropical water similar to that observed along the coast of Peru during El Niño years dominated the northern part of the Benguela Current upwelling system, leading to a temperature increase of 3°C in the upper 50 m of water near 23°S. The causes for such extreme situations in the Atlantic Ocean are not clear. There is also uncertainty about the frequency of their occurrence; only two intrusions of tropical water have been documented for the 40 year period between 1950 and present, although historical records of coastal water temperatures from Namibia seem to indicate one intrusion for every ten years.